Climbing Fiber Activation Induced by Footshock in the Cerebellar Vermis Lobule IV/V of Freely Moving Mice

Rou XUE[1]*, Xiaojing TANG[1]*, Jiechang TANG[1]*, Si ZHANG[1], Xiang LIAO[1], Xiaowei CHEN[2,3], Longhui LI[1], Xingyi LI[1]

** These authors contributed equally to this work.*

[1]Center for Neurointelligence, School of Medicine, Chongqing University, Chongqing, China, [2]Brain Research Center and State Key Laboratory of Trauma, Burns, and Combined Injury, Third Military Medical University, Chongqing, China, [3]Guangyang Bay Laboratory, Chongqing Institute for Brain and Intelligence, Chongqing, China

Received August 6, 2023
Accepted March 12, 2024

Summary

Parallel fibers (PFs) in the cerebellar cortex are involved in a series of coordinated responses in the fear conditioning paradigm induced by footshock. However, whether footshock can activate cerebellar climbing fibers (CFs) remains unclear. In this study, we recorded calcium (Ca^{2+}) activity in CFs by optical fiber photometry in the cerebellar vermis lobule IV/V of freely moving mice with footshock stimulation. We found that the activation of CFs in the lobule IV/V was highly correlated with footshock stimulation but not with the sound stimulation used as a control. This result suggests that afferent information from CFs might be associated with the motor initiation of fear-related behaviors or fear emotion itself. Thus, our results suggest that a characteristic CF signal in the cerebellar cortex might be related to fear processing or footshock-related behaviors (such as startle responses or pain sensation).

Key words

Climbing fibers • Cerebellar lobule IV/V • Footshock • Optical fiber photometry

Corresponding authors

X. Li and L. Li, Center for Neurointelligence, School of Medicine, Chongqing University, Chongqing 400044, China. E-mail: xingyi_li@cqu.edu.cn or E-mail: lilonghui@cqu.edu.cn

Introduction

Fear is an important emotion that arises when an animal encounters a serious threat and can prompt defensive behavior to achieve survival[1]. A series of behavioral paradigms exist for studying fear, of which the footshock paradigm is likely the most classical. Electric footshock at a certain current intensity are used to induce fear-related unconditioned behaviors [2-5]. Studies have shown that the neural circuits involved in fear responses are closely associated with specific brain regions. These regions are mainly the limbic structures such as the amygdala [6,7], the hippocampus [8-10], the midbrain structures such as the periaqueductal gray matter [11], the raphe nuclei [12] and dopaminergic areas [13], the thalamic reticular nucleus[14], the prefrontal cortex [15,16] and the cerebellum [17-20].

The cerebellum is commonly considered the central regulator of somatic balance and the coordinator of random movements [21]. However, it is also involved in fear responses and fear memory processes [17-19]. The cerebellum receives two major afferents, parallel fibers (PFs) as the T-shaped axons of granule cells and climbing fibers (CFs) as the terminals of neurons from the inferior olive (IO), forming numerous synaptic connections with the dendrites of Purkinje cells (PCs) [22,23]. Although it has been demonstrated that synapses between the PCs and the PFs in the cerebellum mediate fear memory processes [17,19], it is unclear whether CFs play a role in fear perception or fear learning processes.

Due to the anatomical location and structure of the cerebellum, it is challenging to apply prevailing

recording techniques in the cerebellar cortex of freely moving animals, especially for recording axonal activities. Despite the technical difficulties, electrophysiological recording achieves high temporal resolution [18,24,25], and two-photon imaging achieves high spatial resolution and recording efficiency [26,27]. However, both techniques are difficult to apply to the cerebellar cortex of freely moving animals. Furthermore, it is challenging to label the axon terminals. Optical fiber photometry through newly emerging genetically encoded calcium indicators (GECIs) can record neural activity in the cerebellar cortex of freely moving mice [28]. We previously reported the successful recording of calcium (Ca^{2+}) activity in the CFs of freely moving mice using this method [29]. Thus, this method allows exploration of the correlation between CFs activities and the fear induced by footshock.

In this study, we hypothesized that CFs, like PFs, plays a role in fear related behaviors. Here, we combined viral tracing technique and immunohistochemistry to verify the projection pattern of IO-lobule IV/V circuit and the effect of the GECIs. Using optical fiber photometry, we recorded the spontaneous Ca^{2+} transients of CFs in lobule IV/V under different anesthesia concentrations, or the induced Ca^{2+} transients with sound or footshock stimulation under freely behaving status. Our results may suggest a new idea for studying the emotional role of the IO-cerebellar circuit. Besides, our study may provide a new perspective for exploring the non-motor function of cerebellum, especially the emotional aspect.

Materials and Methods

Animals

8-week-old male C57BL/6J mice were used [4] in this study. The mice were group-housed in individually ventilated cages (IVC, as home cages) under a 12-h light-dark cycle（light on from 8:00 to 20:00）with food (complete feed) and water ad libitum. The IVC were maintained at a constant temperature (22 °C) and humility (60 %). Before the experiment, the mice were acclimatized in the operating room for at least 30 min after being transferred from the IVC. The experimental operation time was restricted within 8:00-12:00 am. The room temperature (RT) and humidity were set the same as the IVC. All animal experiments complied with the relevant regulations of the Experimental Animal Welfare Ethics Committee of Chongqing University.

Experimental design

There were two main parts of this study (Fig. S1). For morphological verification of the IO-cerebellar circuit, tracers were used to verify the anterograde or retrograde projections of the IO-cerebellar circuit (Fig. 1). Then Cholera Toxin B (CTB) retrograde tracing followed by immunohistochemical staining was applied to confirm the exact projection from IO to lobule IV/V (Fig. 1D). For Ca^{2+} signal recording of the lobule IV/V, the Ca^{2+} signals were recorded under anesthesia (Fig. 2) before the fixation of the optic fiber. Afterwards, Ca^{2+} signals were recorded in freely-moving mice, and comparison of the Ca^{2+} signals during locomotion and grooming behaviors were made (Fig. 3B-E). Finally, comparison of the Ca^{2+} signals under footshock and sound stimulation were made (Fig. 3F-J).

Virus injection

Mice were anesthetized with 2.5 % isoflurane in an acrylic box for 3-5 min, then transferred to the heated plate (37-38 °C) on a stereotaxic apparatus (Zhongshi Technology, Beijing, China), and the head was fixed with a teeth-bar and two ear-bars to ensure stability during the surgery. Ointment was applied to protect the eyes from the surgical light. Then the concentration of isoflurane was reduced to 1.5 % and adjusted in real-time based on the respiratory rate of the mice. The hair was shaved and the skin was disinfected with 1 % iodophor. Afterwards, local infiltration anesthesia was administered with 0.5 % lidocaine, followed by a wait of 3 min before incision. A 2-cm incision was made along the midline of the scalp to expose the skull. Then the surface was cleaned to facilitate the determination of the Bregma and Lambda points (Fig. 2A). The mice skull was made level by adjusting the relevant height of both reference points. A small craniotomy (diameter ~0.5 mm) was made on the skull with a dental drill (bit diameter of 0.45 mm). After the skull fragments was cleaned, virus was delivered to the target brain regions through a pulled glass micropipette (tip diameter of 10-20 μm) at a rate of 50 nl/min using the Nanoject III injector (Drummond Scientific, USA). After injection, the micropipette was kept in position for 10 min to allow the virus to spread. Finally, the scalp was sutured with tissue glue (Vetbond, USA), the isoflurane was turned off to let mice awake, and they were sent back to their home-cage for recovery. Meloxicam (4 mg/kg; Metacam, Germany) was provided subcutaneously on each of the three consecutive days for postoperative analgesia.

For mono-synaptic anterograde tracing of the

olivo-cerebellar circuit, 50 nl tracer AAV2/9-hSyn-EGFP-WPRE-pA (AAV2/9-EGFP) (Taitool Bioscience, Shanghai, China, Cat# S0237-9, Table S1) was injected into the right IO of the mice (anteroposterior (AP): -6.63 mm; mediolateral (ML): +0.35 mm; dorsoventral (DV, below the pia): -5.55 mm, from bregma). For optical fiber recording of the CFs, a new generation of GECIs, the AAV2/9-hSyn-axon-jGCaMP7b-WPRE-pA (AAV2/9-jGCaMP7b, Taitool Bio- science, Shanghai, China, Cat# S0602-9) was applied, which has a 2-times higher sensitivity and 50 % brighter fluorescence than that of GCaMP6s [29]. ('jGCaMP7' means 'Janelia' GCaMP7; 'b' means bright, and is suitable for detecting subcellular neural signals, e.g. dendritic spines and axons.). About 50 nl AAV2/9-jGCaMP7b was injected into the right IO with the parameters above. For retrograde tracing, 100 nl Recombinant Cholera Toxin B subunit-Alexa Fluor™ 555 (CTB 555, Thermo Fisher Scientific, USA, Cat# C22843) or Recombinant Cholera Toxin B subunit-Alexa Fluor™ 647 (CTB 647, Thermo Fisher Scientific, USA, Cat# C34778) were injected into both side of lobule IV/V of the mice (AP: -2.20 mm; ML: ±0.70 mm; DV: 0.70 mm, from lambda). The expression of the tracers in the mouse brains cost 3 weeks for AAV axonal tracing or 1 week for CTB retrograde tracing. Afterwards, mice brains were sampled, fixed and cut into 35 μm or 40 μm slices with freezing microtome (CryoStar NX50, Thermo Fisher Scientific, USA), for axonal tracing or retrograde tracing respectively.

Immunohistochemistry

For sampling the brains, the mice were deeply anesthetized with 1 % pentobarbital sodium (0.1 ml/10 g, Sigma-Aldrich, USA) to ensure no toe-pinching reflex, then perfused intracardially with 0.9 % saline (KELUN, Henan, China) followed by 4 % paraformaldehyde (PFA, Sigma-Aldrich, USA). After perfusion, whole brains were dissected and post-fixed in 15 % sucrose PFA and then dehydrated in 30 % sucrose phosphate-buffered saline (PBS, ZSGB-Bio, Beijing, China). Brains were serially cut at a thickness of 40 μm with freezing microtome (CryoStar NX50, Thermo Fisher Scientific, USA) and the sections were collected in 24 multi-well plates containing 0.1 M PBS. For the first rinse, the sections were washed 3 times (5 min each) on a shaker with a 6-well plate fitted with PBS. Following this, sections were permeabilized with PBS containing 1 % Triton X-100 (1 % PBST, Bio-RAD, USA) at RT for 1 h, and then rinsed again for 3 times (5 min each) in PBS. Next, sections were blocked with a solution of normal donkey serum (Jackson Immunoresearch, USA): 1 % PBST: 0.1 M PBS (ratio 1:3:6) for 2 h at RT in the dark, and then were incubated in thermostat water bath (JingQi, Shanghai, China) for 2 h at 37 °C with primary antibody solution in 0.3 % PBST. Primary antibody used was rabbit anti-Calbindin D-28K (1:250, Sigma-Aldrich, USA, Cat# ZRB1778). After washing 5 times for 10 min in PBS, the secondary antibody, Alexa Fluor 488 Donkey Anti-Rabbit IgG (1:1000, Invitrogen, USA, Cat# A-21206), was used for 2 h at RT in the dark. Sections were again washed 5 times for 10 min in PBS and stained with 4',6-diamidino-2-phenylindole (DAPI, 1:1000, Sigma-Aldrich, USA, Cat# D9542) for 8 min at RT in the dark. Finally, rinsed 5 times again with PBS, then mounted onto the microscope slides for fluorescence imaging.

Optical fiber setup

The optical fiber setup adopts Dual-Channel Fiber Photometry (Thinker Tech Nanjing Biotech Co., Ltd., Nanjing, China) and supporting analysis software, in which the blue light excitation light wavelength was 470 nm, and the yellow light excitation light wavelength was 594 nm. The emitted light from the blue and yellow light sources was combined into a single beam through a dichroic mirror and coupled into the same multimode fiber (200 μm diameter, 0.37 Numerical Aperture (NA), Inper, Zhejiang, China) after convergence by the objective lens (Fig. 2A). In this experiment, the CFs labeled by the jGCaMP7b emitted green fluorescence under blue light excitation, which was converted by the detector into electrical signals to represent the neural activity, and the yellow light was used as a control group to monitor motor artifacts.

Optical fiber recording in anesthetized mice

To evaluate the capacity of the GECIs and report the changing CF signals in the cerebellar cortex, we recorded changes in fluorescence intensity in the lobule IV/V in mice under different levels of anesthesia (Fig. 2). The optical fiber was glued with a cannula (inner diameter 0.57 mm, outer diameter 0.81 mm), and the tip was extended 0.9 mm from the cannula. Then, the optical fiber was placed above the craniotomy over the left lobule IV/V with a holder (Fig. 2A). The tip was advanced to the dura surface to achieve maximum fluorescence stability. The cranial window was kept moist with 0.1 M PBS during recording. The concentration of isoflurane was initially set at 0.6 % and was increased gradually to 1.0 %, then to 1.2 %, and finally to 1.4 % (Fig. 2D). At each concentration, the

mice were adapted for 20 min, and when their respiration rates were stable (consistent respiratory rate observed on three consecutive observations separated by at least 1 min), spontaneous Ca^{2+} transients were recorded for 10 min. In the control group, AAV2/9-EGFP was injected into unilateral IO, and the optic fiber was implanted in lobule IV/V. The real time-fluorescence changes were recorded under 0.6 % isoflurane anesthesia to eliminate motion artifact.

Optical fiber recording in freely moving mice

To explore the response of the cerebellar CFs to footshock in freely moving mice, we performed optical fiber implantation in lobule IV/V of the cerebellum to facilitate long-term behavioral observations and recordings (Fig. 3A). After confirming Ca^{2+} signals under anesthesia, the optical fiber was fixed at the site with dental cement, which was then air-dried and coated with black pigment to prevent light interference. The mice were then moved to the laboratory bucket with optical fiber for 5 days of recovery (Fig. 2A). During the recording, the mice were placed in a 60 cm × 60 cm open field (Fig. 3B), and the optical fiber was connected to the recording system. The signal light was manually triggered and the recording of the Ca^{2+} signals started simultaneously with sound or footshock stimuli that were conducted at a programmed time. Thus, the first frame with the signal light on was aligned with the trigger point (a square wave in another channel synchronized with the recording channel) to synchronize the behavioral video with the Ca^{2+} signals. On the 6^{th} day of recovery, Ca^{2+} signal was recorded for 15 min in freely moving mice, and then sound stimulation (pure tone of 8944 Hz, 75 dB, 10 times 1 s each, trial interval 180 s) was applied and the Ca^{2+} signal was also recorded (Fig. 3F). Afterwards, the mice were sent back to its bucket and allowed to rest for 24 h. On the following day (7^{th} day), the mice were placed in a 60 cm × 60 cm footshock box (Fig. 3F). After an adaptation period of 3 min, the footshock stimulation was applied (0.6 mA, 10 times 1 s each, trial interval 180 s) and the Ca^{2+} signal was recorded. During the recording, the camera captured all the behavior processes of mice and the light flash marker, and the behavior and Ca^{2+} signals were analyzed synchronously offline.

Data analysis

The sampling rate of the optical fiber system was 100 Hz, and the camera shooting frequency was 30 Hz. The Labview optical fiber data analysis program was used to perform Savitzky-Golay finite pulse smoothing filtering on the raw Ca^{2+} signal with 15 side points and 3 polynomial orders. For the freely moving mouse Ca^{2+} signal data, the first frame with the signal light on was aligned with the first frame of the wave above the Ca^{2+} signal to synchronize the behavior with the signal. For mouse sound stimulation and footshock stimulation Ca^{2+} signal data, the signal analysis was performed directly on the basis of the fixed intervals of the square waves for specific events (sound and footshock). The Ca^{2+} signal amplitude was determined according to $\Delta F/F= (f - f_{baseline})/f_{baseline}$, and we defined spikes three times larger than the standard deviation of the baseline amplitude as Ca^{2+} signal events. Statistical analysis of frequency and amplitude under different anesthetic concentrations was performed using the Brown-Forsythe and Welch ANOVA test, the Ordinary one-way ANOVA test, and the remaining Ca^{2+} signals were analyzed using a Mann-Whitney U test. Then, plotted as the mean ± S.E.M. in graphs. Analysis was performed using Labview, Graphpad (Prism) or MATLAB (Mathworks). Statistical significance was defined as **** $P<0.0001$, *** $P<0.001$, ** $P<0.01$, * $P<0.05$.

Results

Validation of the contralateral projection pattern of the olivo-cerebellar circuit

To demonstrate the projection pattern from the IO to the cerebellar cortex, we injected the virus AAV2/9-EGFP into the IO and confirmed *via post hoc* histology that the tracer was confined to the IO and did not spread to other regions (Fig. 1A). AAV2/9-EGFP was specifically expressed in the contralateral CFs, and its continuous lateral-to-medial distribution pattern was confirmed with serial tissue sections (Fig. 1B). The CFs originate from the IO, with the main pathway contralateral to the spinal trigeminal tract and inferior cerebellar peduncle and terminating in the molecular layer of the cerebellar cortex. In addition, the retrograde tracing from both sides of the lobule IV/V to the IO showed the result that CTB 555 and CTB 647 were restricted to the respective injection side in the lobule IV/V (Fig. 1C). The cyan or red dyes were specifically expressed on either side of the lobule IV/V and traced back to the contralateral IO neurons, which were predominantly distributed in the sub-region dorsal inferior olive (IOD, Fig. 1D).

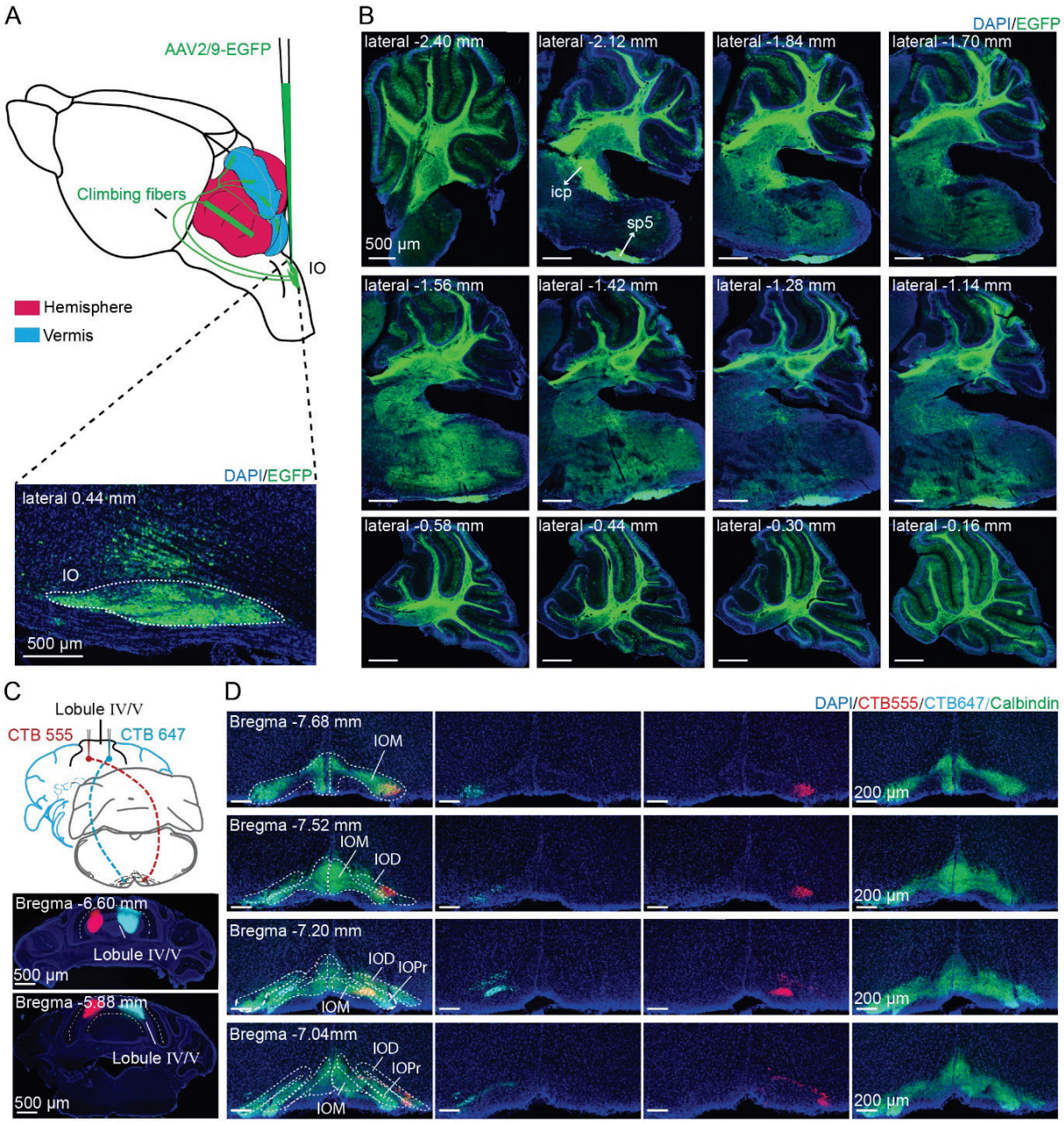

Fig. 1. Verification of the projection pathway of the IO-cerebellar cortex. (**A**) Scheme of anterograde injection of the virus into the IO. Upper panel, the scheme of anterograde injection of the virus AAV2/9-hSyn-EGFP-WPRE-pA into the IO. Lower panel, the merged fluorescence image result of the viral injection. Scale bar=500 μm. (**B**) A series of sagittal fluorescence images (thickness=35 μm) of the contralateral cerebellum. CFs labeled by enhanced green fluorescent protein (EGFP) across icp and sp5 are distributed in almost all contralateral cerebellar lobules. The acquisition range of brain sections is -0.16 – -2.40 mm (relative to midline). Scale bar=500 μm. icp, the inferior cerebellar peduncle; sp5, spinal trigeminal tract. n=5 mice. (**C**) Upper panel, the scheme of CTB555/647 injection into the vermis IV/V. Lower panel, the merged fluorescence image result of the CTB555/647 injection. Scale bar=500 μm. n=5 mice. (**D**) A series of coronal fluorescence images of the IO (thickness=40 μm), where red and cyan fluorescence represent neurons retrogradely projecting from the bilateral vermis IV/V back to the IO. Scale bar=200 μm. IOM, medial inferior olive; IOD, dorsal inferior olive; IOPr, principal inferior olive. n=5 mice.

Recording of CF Ca^{2+} signals under different anesthesia levels

The results showed that the frequency of CF Ca^{2+} transients was influenced by anesthesia levels (0.6 %, 1.0 %, 1.2 %, and 1.4 % isoflurane concentration; Fig. 2D). As the isoflurane concentration increased, the frequency decreased from 0.37±0.05 Hz to 0.006±0.005 Hz (Fig. 2F). There is significant difference between the lowest and the highest dose (Brown-Forsythe and Welch ANOVA test, ** P=0.0012). However, the amplitude (ΔF/F) of the CF Ca^{2+} transients was not significantly affected by the changes in the anesthesia

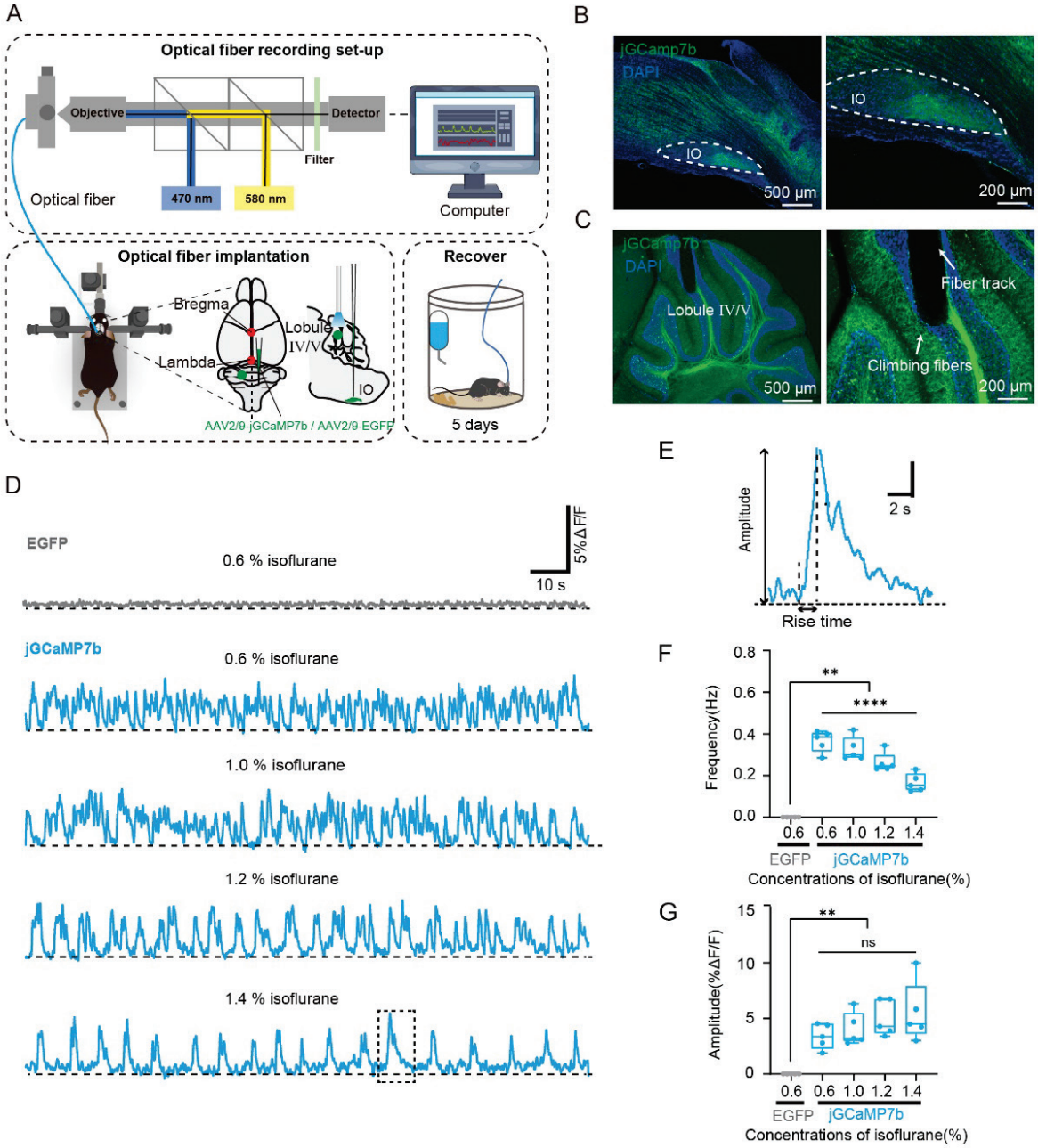

Fig. 2. Population Ca^{2+} recording of CFs in anesthetized mice injected with jGCaMP7b. (**A**) Schematic of optical fiber recording under anesthesia and postoperative recovery in mice. In the bottom left panel, the red points represent the reference points Bregma and Lambda and the green points represent the fiber implantation site in lobule IV/V. The sagittal section showed that Ca^{2+} indicator AAV2/9-jGCaMP7b or tracer AAV2/9-EGFP were injected into IO to label CFs. (**B**) Left: Result of jGCaMP7b labeling in the IO. Scale bar=500 μm. Right: Left image zoomed-in. Scale bar=200 μm. (**C**) Left: Morphological results of the fiber tract in the lobule IV/V. Scale bar=500 μm. Right: Left image zoomed-in. Scale bar=200 μm. (**D**) Examples showing the change in fluorescence (ΔF/F) over time in lobule IV/V in a mouse injected with control AAV2/9-EGFP (gray) and an experimental mouse injected with AAV2/9-jGCaMP7b (blue) expressing Ca^{2+} indicator. Signals were collected for different concentrations of isoflurane (0.6 %, 1.0 %, 1.2 %, and 1.4 %). (**E**) Example Ca^{2+} transient shows rise time and amplitude. (**F**) Frequency of CF Ca^{2+} signals in lobule IV/V for different concentrations of isoflurane (Between experimental groups: Brown-Forsythe and Welch ANOVA test, **** P<0.0001; between control groups with experimental groups: Mann-Whitney test, ** P=0.0079<0.01, n=5 mice). (**G**) Amplitude of CF Ca^{2+} signals in lobule IV/V for different concentrations of isoflurane (Between experimental groups: Ordinary one-way ANOVA test, P=0.293; between control groups with experimental groups: Mann-Whitney test, ** P=0.0079<0.01, n=5 mice).

level (Fig. 2G). Under the same anesthesia level (0.6 %) and recording position, the frequency (Fig. 2F) and amplitude (Fig. 2G) of Ca^{2+} signals in the CFs of the control group (AAV2/9-EGFP) were significantly lower than those in the experimental group (AAV2/9-jGCaMP7b), indicating that the changes in fluorescence in the jGCaMP7b group were not a consequence of movement or breathing artifacts.

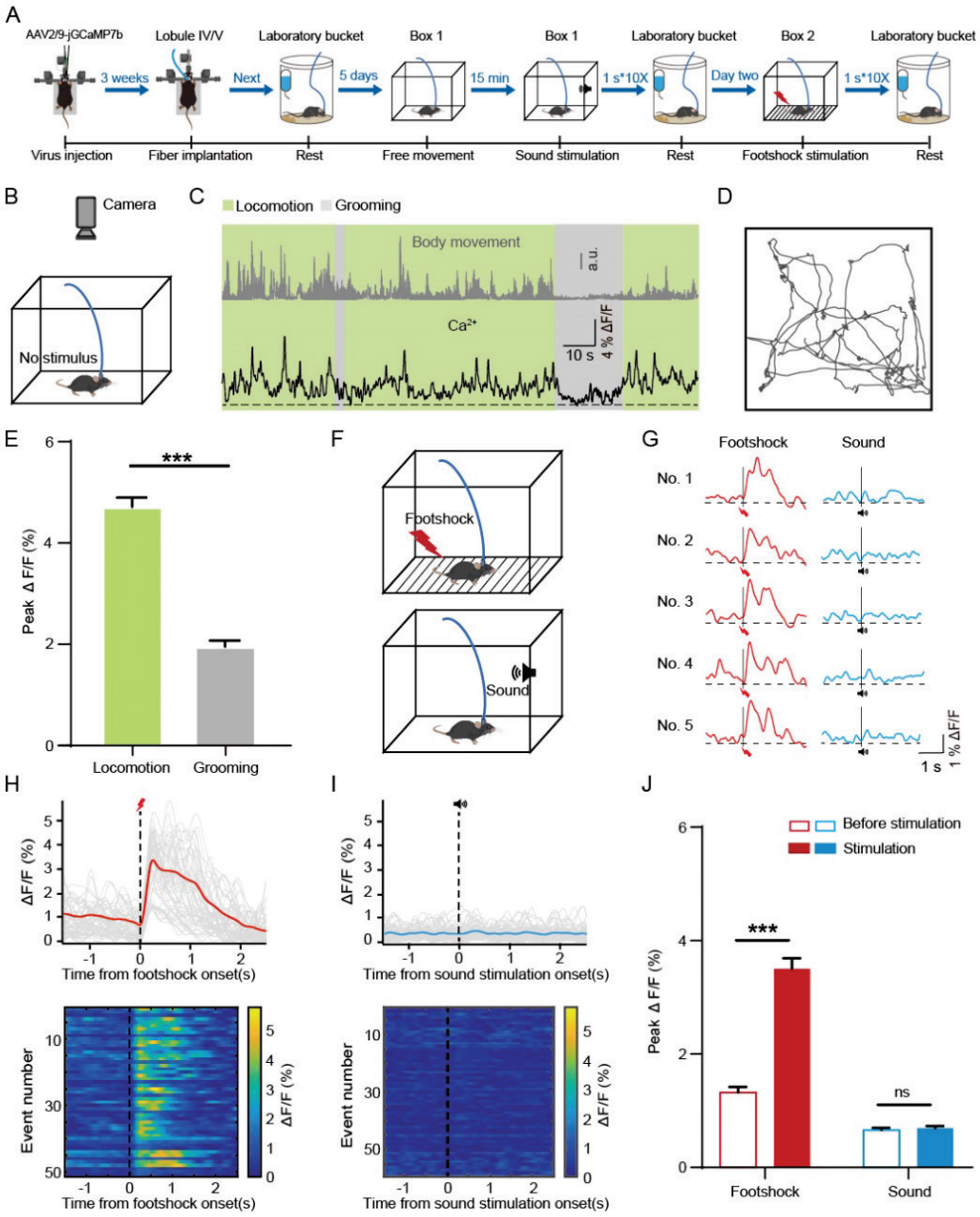

Fig. 3. Population Ca^{2+} transients of CFs induced by footshock stimulation in freely moving mice. (**A**) Flow chart of footshock experiment. (**B**) Diagram of the recording setup in freely moving mice. (**C**) Example showing the relative body movements (gray trace) and the Ca^{2+} transients recorded in CFs (black trace) in a freely moving mouse; gray-shaded areas: grooming; green-shaded areas: locomotion. (**D**) Corresponding locomotion trajectory of the recording period in C. (**E**) Summary of peak ΔF/F during locomotion or grooming (locomotion: n=68 trials from 6 mice; grooming: n=42 trials from 6 mice, Mann-Whitney U test, Z=-8.045, *** P<0.001). (**F**) Schematic diagram of Ca^{2+} recording with footshock or sound stimulation. (**G**) Representative Ca^{2+} signals induced after footshock (red) or sound (blue) in CFs from one mouse. (**H, I**) Average trace (top) and heat map (bottom) of Ca^{2+} signals aligned to footshock (H, n=51 trials from 6 mice) or sound (I, n=59 trials from 6 mice) stimulation. The gray lines represent each event. (**J**) Summary of peak ΔF/F 1 s before and during footshock and sound stimulation (footshock: n=51 trials from 6 mice, sound: n=59 trials from 6 mice, Mann-Whitney U test, before footshock vs. footshock, Z=-9.361, *** P<0.001; before sound vs. sound, Z=-0.921, P=0.357).

Cluster Ca^{2+} signaling response in CFs evoked by footshock in freely moving mice

The mice were placed in an open field for free movement, and the Ca^{2+} signals were recorded for 15 min (Fig. 3B). We selected a period of 200 s with locomotion and grooming for the simultaneous analysis of body movements and Ca^{2+} signals (Fig. 3C); the activity trajectory of the mice during the selected period was plotted retrospectively (Fig. 3D). The statistical analysis revealed that the Ca^{2+} signal amplitude during locomotion was significantly higher than that during grooming (Fig. 3E). Next, the mice were subjected to a fixed

frequency and duration of sound stimulation or electric stimulation (Fig. 3F), and it was found that the sound stimulation hardly elicited a typical Ca^{2+} signal (Fig. 3G, blue lines), whereas footshock stimulation elicited strong CFs activities (Fig. 3G, red lines). Statistical analysis revealed that the amplitude of the Ca^{2+} transients in CFs induced by footshock was significantly higher than the baseline before footshock (Fig. 3J, red), while the Ca^{2+} transient amplitude of sound-induced CFs was not different from the baseline before sound (Fig. 3J, blue).

Discussion

In this study, we used optical fiber photometry combined with GECIs to record Ca^{2+} signals in the CFs of lobule IV/V in anesthetized or freely moving mice. Under anesthesia, the amplitude and frequency of Ca^{2+} signals in the CFs differed among isoflurane concentrations (Fig. 2F, G). In awake mice, the CFs Ca^{2+} signal was significantly higher when the mice were free to explore than when the mice were relatively stationary, such as grooming (Fig. 3C, E). It was shown that the baseline of footshock (~1 %) was higher than that of sound (~0.5 %) (Fig. 3J). As the fiber photometry represents populational activity rather than single-cell activity, it was suggested that there might be higher motion intensity with footshock than that with sound. After the administration of a footshock, the CFs exhibited stable Ca^{2+} signals with significantly higher amplitude relative to the baseline (Fig. 3J, red), whereas sound stimulation failed to elicit such a strong response (Fig. 3J, blue). It is suggested that the CFs could be strongly activated by footshock, which was assumed as a characteristic fear-related stimuli. Here, we propose three possible speculations to explain the strong response of the CFs to fear-related stimuli. First, CF activities to the footshock may be an instructor of the consequent defensive behaviors responding to the frightening stimuli. From this perspective, the pain caused by the footshock might trigger the survival circuits through the olivo-cerebellar system [29]. Second, CF activities certainly activated the CF-PC synapses, which occurred simultaneously with the activation of the PF-PC synapses during fear conditioning [17,19]. It is inferred that the CFs contribute to cerebellar fear learning or memory consolidation similar to the PFs. Third, as the motion of the mice induced by footshock is more intense than that of sound, it is not negligible that the stronger motor could also be a potential factor in causing population Ca^{2+} transients of CFs. Therefore, further studies are needed to elucidate whether the signal is a sensory afferent (pain or fear) or a motor afferent (shock-induced defensive behavior) and whether the signal represents a communication of information or a correction of behavior.

The greatest advantage of this research compared with that of others is that it solves the problem of limited animal behavior in previous studies on the cerebellum *via* optical fiber photometry. In addition, the classical theory of cerebellar motor learning suggests that CFs from the IO transmit the necessary training information to the cerebellar cortex to guide the cerebellum in learning [31,32]. Therefore, previous studies have often focused on the role of CFs in motor learning [33-35]. In contrast, studies on fear memory and fear conditioning focused on the cerebellum have also assessed the synapses formed by PFs and PCs in freely moving mice. The firing mechanisms of CFs in response to fear stimuli have been poorly studied in freely moving mice. Since electrophysiological experiments were performed on isolated brain slices, the role of CF-PC synapses in the fear acquisition phase cannot be ruled out [18]. Our study complements this shortcoming in cerebellar research and provides new research ideas for studying non-motor functions in the cerebellum. However, there are several shortcomings in this study, such as the lack of using the electrophysiological or two-photon imaging techniques with high temporal and spatial resolution. And the optic fiber recording of clustered Ca^{2+} signals might have a low signal-to-noise ratio, which will inevitably miss part of the neuronal firing information during the signal analysis. The effect of motor activity could not be filtered either, and further studies with higher spatial temporal resolution might be needed to verify whether the involvement of motor activity induced by footshock in mice disturbs the population Ca^{2+} transients of CFs. In addition, this study only recorded Ca^{2+} signals from CFs under fear stimulation conditions, and future work is needed to investigate the role of CFs in fear learning in depth.

The cerebellum is an important component of a topologically structured and functionally rich brain. Classically, the olive-cerebellar circuit is considered a real-time error calculation system that continuously corrects executed actions by calculating the error between the sensory information (feedforward) and the motor information (feedback) transmitted by CFs through a highly organized and preserved network of cells [33,36]. The olivo-cerebellar system greatly contributes

to the multi-faced functions of the cerebellum, including the classical functions of maintaining balance [37], coordinating movement [38], and regulating muscle tone [39], as well as cognitive functions [40,41] and food intake [42]. Our study reveals that the olivo-cerebellar system also plays a role in the emotional function of the cerebellum, which may bring more attention to the study of the cerebellum function that influences emotions [43]. Combining optic fiber recording with specific GECI labeling, our approach allowed Ca^{2+} signal recording in freely moving mice during conventional fear stimulation, and could be expanded in future studies by combining it with other prevailing techniques, such as chemogenetic manipulation. The method established in this study and the experimental ideas presented demonstrate the potential for the discovery of more cerebellum functions based on the olivo-cerebellar circuits. The study of the emotional cerebellum should also provide new therapeutic ideas and targets for many mood disorders, such as post-traumatic stress disorder [44,45], autism [46], and schizophrenia [47].

Conflict of Interest

There is no conflict of interest.

Acknowledgements

We are grateful to Zhiqi Yang, Han Qin and Zhehao Xu for very helpful discussions and comments, and to Hong Qu for technical assistance. We thank the LetPub Inc. for providing language editing. This research was funded by the National Natural Science Foundation of China to X. C., grant number 32127801; the Chongqing Postdoctoral Science Special Foundation to X.L., grant number 2019LY18.

References

1. Tovote P, Fadok JP, Luthi A. Neuronal circuits for fear and anxiety. Nat Rev Neurosci 2015;16:317-331. https://doi.org/10.1038/nrn3945
2. Zhang K, Forster R, He W, Liao X, Li J, Yang C, Qin H, ET AL. Fear learning induces alpha7-nicotinic acetylcholine receptor-mediated astrocytic responsiveness that is required for memory persistence. Nat Neurosci 2021;24:1686-1698. https://doi.org/10.1038/s41593-021-00949-8
3. Colon LM, Poulos AM. Contextual processing elicits sex differences in dorsal hippocampus activation following footshock and context fear retrieval. Behav Brain Res 2020;393:112771. https://doi.org/10.1016/j.bbr.2020.112771
4. Huang W, Qin J, Zhang C, Qin H, Xie P. Footshock-induced activation of the claustrum-entorhinal cortical pathway in freely moving mice. Physiol Res 2022;71:695-701. https://doi.org/10.33549/physiolres.934899
5. Zelenka O, Novak O, Brunova A, Syka J. Heterogeneous associative plasticity in the auditory cortex induced by fear learning - novel insight into the classical conditioning paradigm. Physiol Res 2021;70:447-460. https://doi.org/10.33549/physiolres.934559
6. Sun Y, Gooch H, Sah P. Fear conditioning and the basolateral amygdala. F1000Res 2020;9:F1000. https://doi.org/10.12688/f1000research.21201.1
7. Gallagher M, Chiba AA. The amygdala and emotion. Curr Opin Neurobiol 1996;6:221-227. https://doi.org/10.1016/S0959-4388(96)80076-6
8. Chaaya N, Battle AR, Johnson LR. An update on contextual fear memory mechanisms: Transition between Amygdala and Hippocampus. Neurosci Biobehav Rev 2018;92:43-54. https://doi.org/10.1016/j.neubiorev.2018.05.013
9. Bian X-L, Qin C, Cai C-Y, Zhou Y, Tao Y, Lin Y-H, Wu H-Y, ET AL. Anterior Cingulate Cortex to Ventral Hippocampus Circuit Mediates Contextual Fear Generalization. J Neurosci 2019;39:5728-5739. https://doi.org/10.1523/JNEUROSCI.2739-18.2019
10. Liberzon I, Martis B. Neuroimaging studies of emotional responses in PTSD. Ann N Y Acad Sci 2006;1071:87-109. https://doi.org/10.1196/annals.1364.009
11. Walker RA, Wright KM, Jhou TC, McDannald MA. The ventrolateral periaqueductal grey updates fear via positive prediction error. Eur J Neurosci 2020;51:866-880. https://doi.org/10.1111/ejn.14536
12. Silva RCB, Cruz APM, Avanzi V, Landeira-Fernandez J, Brandão ML. Distinct contributions of median raphe nucleus to contextual fear conditioning and fear-potentiated startle. Neural Plast 2002;9:233-247. https://doi.org/10.1155/NP.2002.233

13. Small KM, Nunes E, Hughley S, Addy NA. Ventral tegmental area muscarinic receptors modulate depression and anxiety-related behaviors in rats. Neurosci Lett 2016;616:80-85. https://doi.org/10.1016/j.neulet.2016.01.057
14. Dong P, Wang H, Shen XF, Jiang P, Zhu X-T, Li Y, Gao J-H, ET AL. A novel cortico-intrathalamic circuit for flight behavior. Nat Neurosci 2019;22:941-949. https://doi.org/10.1038/s41593-019-0391-6
15. Dixsaut L, Graff J. The Medial Prefrontal Cortex and Fear Memory: Dynamics, Connectivity, and Engrams. Int J Mol Sci 2021;22:12113. https://doi.org/10.3390/ijms222212113
16. Ji G, Neugebauer V. Modulation of medial prefrontal cortical activity using in vivo recordings and optogenetics. Mol Brain 2012;5:36. https://doi.org/10.1186/1756-6606-5-36
17. Sacchetti B, Scelfo B, Tempia F, Strata P. Long-term synaptic changes induced in the cerebellar cortex by fear conditioning. Neuron 2004;42:973-982. https://doi.org/10.1016/j.neuron.2004.05.012
18. Lawrenson C, Paci E, Pickford J, Drake RAR, Lumb BM, Apps R. Cerebellar modulation of memory encoding in the periaqueductal grey and fear behaviour. Elife 2022;11:e76278. https://doi.org/10.7554/eLife.76278
19. Sacchetti B, Scelfo B, Strata P. The cerebellum: synaptic changes and fear conditioning. Neuroscientist 2005;11:217-227. https://doi.org/10.1177/1073858405276428
20. Strata P, Scelfo B, Sacchetti B. Involvement of cerebellum in emotional behavior. Physiol Res 2011;60(Suppl 1):S39-S48. https://doi.org/10.33549/physiolres.932169
21. Fine EJ, Ionita CC, Lohr L. The history of the development of the cerebellar examination. Semin Neurol 2002;22:375-384. https://doi.org/10.1055/s-2002-36759
22. Watanabe M. Molecular mechanisms governing competitive synaptic wiring in cerebellar Purkinje cells. Tohoku J Exp Med 2008;214:175-190. https://doi.org/10.1620/tjem.214.175
23. Ito M. Historical review of the significance of the cerebellum and the role of Purkinje cells in motor learning. Ann N Y Acad Sci 2002;978:273-288. https://doi.org/10.1111/j.1749-6632.2002.tb07574.x
24. Woodruff-Pak DS, Foy MR, Akopian GG, Lee KH, Zach J, Nguyen KPT, Comalli DM, ET AL. Differential effects and rates of normal aging in cerebellum and hippocampus. Proc Natl Acad Sci U S A 2010;107:1624-1629. https://doi.org/10.1073/pnas.0914207107
25. Frontera JL, Baba Aissa H, Sala RW, Mailhes-Hamon C, Georgescu IA, Léna C, Popa D. Bidirectional control of fear memories by cerebellar neurons projecting to the ventrolateral periaqueductal grey. Nat Commun 2020;11:5207. https://doi.org/10.1038/s41467-020-18953-0
26. Chen X, Kovalchuk Y, Adelsberger H, Henning HA, Sausbier M, Wietzorrek G, Ruth P, ET AL. Disruption of the olivo-cerebellar circuit by Purkinje neuron-specific ablation of BK channels. Proc Natl Acad Sci U S A 2010;107:12323-12328. https://doi.org/10.1073/pnas.1001745107
27. Wagner MJ, Savall J, Hernandez O, Mel G, Inan H, Rumyantsev O, Lecoq J, ET AL. A neural circuit state change underlying skilled movements. Cell 2021;184:3731-3747. https://doi.org/10.1016/j.cell.2021.06.001
28. Kim OA, Ohmae S, Medina JF. A cerebello-olivary signal for negative prediction error is sufficient to cause extinction of associative motor learning. Nat Neurosci 2020;23:1550-1554. https://doi.org/10.1038/s41593-020-00732-1
29. Tang J, Xue R, Wang Y, Li M, Jia H, Pakan JMP, Li L, ET AL. Optical Fiber-Based Recording of Climbing Fiber Ca2+ Signals in Freely Behaving Mice. Biology (Basel) 2022;11:907. https://doi.org/10.3390/biology11060907
30. Watson TC, Koutsikou S, Cerminara NL, Flavell CR, Crook JJ, Lumb BM, Apps R. The olivo-cerebellar system and its relationship to survival circuits. Front Neural Circuits 2013;7:72. https://doi.org/10.3389/fncir.2013.00072
31. Berthier NE, Singh SP, Barto AG, Houk JC. Distributed representation of limb motor programs in arrays of adjustable pattern generators. J Cogn Neurosci 1993;5:56-78. https://doi.org/10.1162/jocn.1993.5.1.56
32. Pritchett DL, Carey MR. A matter of trial and error for motor learning. Trends Neurosci 2014;37:465-466. https://doi.org/10.1016/j.tins.2014.08.001
33. Marr D. A theory of cerebellar cortex. J Physiol 1969;202:437-470. https://doi.org/10.1113/jphysiol.1969.sp008820
34. Zang Y, De Schutter E. Climbing Fibers Provide Graded Error Signals in Cerebellar Learning. Front Syst Neurosci 2019;13:46. https://doi.org/10.3389/fnsys.2019.00046
35. Ito M. Neural design of the cerebellar motor control system. Brain Res 1972;40:81-84. https://doi.org/10.1016/0006-8993(72)90110-2

36. Albus JS. A theory of cerebellar function. Math Biosci 1971;10:25-61. https://doi.org/10.1016/0025-5564(71)90051-4
37. Barmack NH, Pettorossi VE. Adaptive Balance in Posterior Cerebellum. Front Neurol 2021;12:635259. https://doi.org/10.3389/fneur.2021.635259
38. Thach WT, Goodkin HP, Keating JG. The cerebellum and the adaptive coordination of movement. Annu Rev Neurosci 1992;15:403-442. https://doi.org/10.1146/annurev.ne.15.030192.002155
39. Manni E, Petrosini L. Luciani's work on the cerebellum a century later. Trends Neurosci 1997;20:112-116. https://doi.org/10.1016/S0166-2236(96)10077-1
40. Koziol LF, Budding D, Andreasen N, D'Arrigo S, Bulgheroni S, Imamizu H, Ito M, ET AL. Consensus paper: the cerebellum's role in movement and cognition. Cerebellum 2014;13:151-177. https://doi.org/10.1007/s12311-013-0511-x
41. Schmahmann JD, Sherman JC. The cerebellar cognitive affective syndrome. Brain 1998;121:561-579. https://doi.org/10.1093/brain/121.4.561
42. Low AYT, Goldstein N, Gaunt JR, Huang K-P, Zainolabidin N, Yip AKK, Carty JRE, ET AL. Reverse-translational identification of a cerebellar satiation network. Nature 2021;600:269-273. https://doi.org/10.1038/s41586-021-04143-5
43. Bastian AJ. Moving, sensing and learning with cerebellar damage. Curr Opin Neurobiol 2011;21:596-601. https://doi.org/10.1016/j.conb.2011.06.007
44. Preston G, Emmerzaal T, Radenkovic S, Lanza IR, Oglesbee D, Morava E, Kozicz T. Cerebellar and multi-system metabolic reprogramming associated with trauma exposure and post-traumatic stress disorder (PTSD)-like behavior in mice. Neurobiol Stress 2021;14:100300. https://doi.org/10.1016/j.ynstr.2021.100300
45. Holmes SE, Scheinost D, DellaGioia N, Davis MT, Matuskey D, Pietrzak RH, Hampson M, ET AL. Cerebellar and prefrontal cortical alterations in PTSD: structural and functional evidence. Chronic Stress (Thousand Oaks) 2018;2:2470547018786390. https://doi.org/10.1177/2470547018786390
46. Wang SS, Kloth AD, Badura A. The cerebellum, sensitive periods, and autism. Neuron 2014;83:518-532. https://doi.org/10.1016/j.neuron.2014.07.016
47. Mothersill O, Knee-Zaska C, Donohoe G. Emotion and Theory of Mind in Schizophrenia-Investigating the Role of the Cerebellum. Cerebellum 2016;15:357-368. https://doi.org/10.1007/s12311-015-0696-2